INTERNATIONAL JOURNAL FOR NUMERICAL METHODS IN FLUIDS
Int. J. Numer. Meth. Fluids 2009; **59**:1203–1216
Published online 30 July 2008 in Wiley InterScience (www.interscience.wiley.com). DOI: 10.1002/fld.1868

A computational study of gas flow in a De-Laval micronozzle at different throat diameters

C. X. Lin[1,*,†] and V. V. V. Gadepalli[2]

[1]*Department of Mechanical, Aerospace and Biomedical Engineering, The University of Tennessee, Knoxville, TN 37996, U.S.A.*
[2]*University of Phoenix, Phoenix AZ 85040, U.S.A.*

SUMMARY

A numerical study has been carried out to investigate the gas flows in a micronozzle using a continuum model under both slip and no-slip boundary conditions. The governing equations were solved with a finite volume method. The numerical model was validated with available experimental data. Numerical results of exit thrust showed good agreement with experimental data except at very low Reynolds numbers. For parametric studies on the effect of geometric scaling, the nozzle throat diameter was varied from 10 to 0.1 mm, whereas throat Reynolds number was varied from 5 to 2000. A correlation has also been developed to calculate the specific impulse at specified throat diameter and Reynolds number. The effect of different gases on the specific impulse of the nozzle, such as helium, nitrogen, argon and carbon dioxide, was also examined. Copyright © 2008 John Wiley & Sons, Ltd.

Received 24 November 2007; Revised 8 May 2008; Accepted 25 May 2008

KEY WORDS: nozzle flow; micronozzle; gas flow; subsonic flow; finite volume method; computational fluid dynamics

1. INTRODUCTION

In the development of modern space systems, the interest in reducing mass and dimension has resulted in the increased efforts in the study of micro propulsion systems. Advanced micro propulsion systems for micro and nano satellite applications are becoming more and more important to national defense and aerospace industries. In general, the masses of these micro satellites are in the range of 1–50 kg, requiring a thrust value of 0.19 mN [1]. These propulsion systems require

*Correspondence to: C. X. Lin, Department of Mechanical, Aerospace and Biomedical Engineering, The University of Tennessee, Knoxville, TN 37996, U.S.A.
†E-mail: lincx@utk.edu

Contract/grant sponsor: Air Force Office of Scientific Research (AFOSR); contract/grant number: F49620-03-1-0314

very low thrusts for accurate orbital maneuvering and positioning. Some of the key components in these systems that can produce low thrusts include micronozzles and orifices.

Rothe [1] conducted experiments to study the internal and external flows in a supersonic nozzle using the electron beam technique. In his study, the nozzle had a throat diameter of 5.1 mm and nitrogen was used as the test gas. Ivanov *et al.* [2] evaluated the performance of two-dimensional micro nozzle for helium flow using both Navier–Stokes (N-S) equations and direct simulation Monte Carlo (DSMC) methods at $Re_{\text{throat}} = 1$–160. Two nozzle geometries were studied with inlet angles of 54.7 and 30°, and a diverging angle of 15°. Kim [3] using a full N-S code studied the effect of viscous and divergence losses on the performance of a resistojet nozzle. Three configurations of the nozzles were studied, which include outlet angles of 20, 30° and contoured wall at $Re_{\text{throat}} = 1150$, with 0.15 MPa chamber pressure and 1500 K chamber temperature. Chung *et al.* [4] investigated the low-density gas flows in a convergent–divergent nozzle using DSMC and continuum code. The continuum code solved N-S equations by the lower–upper symmetric successive over-relaxation scheme (LU-SSOR). Predictions using both approaches were found to be in good agreement with the experimental results of Rothe [1]. The effect of wall contour on the performance of the nozzle flows was studied numerically by Zeleznik *et al.* [5] and Choudhuri *et al.* [6]. Zeleznik *et al.* [5] investigated the loss mechanism involved in conical, trumpet-shaped and bell-shaped nozzles for heated and unheated flows using nitrogen as the test propellant. Choudhuri *et al.* [6] used color schlieren deflectometry for experimental studies of micronozzle. Boyd *et al.* [7] carried out both experimental and numerical studies on nitrogen flow in a small nozzle expansion at vacuum conditions. In their numerical predictions two different approaches, continuum approach and DSMC, were adopted. Comparison of numerical and experimental data has shown that DSMC technique is superior for prediction of expanding flow.

In the microscale—in terms of throat diameter—Bayt [8] studied the viscous effects in supersonic MEMS-fabricated micronozzles. Numerical investigations were carried out to compare the performance of micronozzles having an expansion ratio of 7.1:1 and different divergence angles (15, 20, 30°). It was found that exit thrust decreases marginally with increasing expansion angle due to dominance of divergence losses. Menzies *et al.* [9] have verified the finding of two-dimensional computation and experiments by Bayt [8]. They have also investigated its extant to the three dimension problem. Rossi *et al.* [10] introduced a model on computation of unsteady flow in micro-thruster with no-slip boundary conditions. The nozzle had a throat diameter of 0.894 mm. Raju *et al.* [11] extended the work of Rossi *et al.* [10] in a two-dimensional finite element formulation for both no-slip and slip flows. Their results [11] of no-slip flow were found almost identical with that of Rossi *et al.* [10] while the thrust value was 44% higher. Ivanov *et al.* [12] performed multi-zone computational modeling of the gas flows in the plumes of micronozzles and orifices, with continuum flow using N-S equations, transitional flows using DSMC and free molecular flows using test particle Monte Carlo (TPMC). Jamison and Ketsdever [13] conducted experiments to evaluate the performance of underexpanded orifice and typical conical nozzles. In their experiments, stagnation pressure was maintained up to 17 torr at a stagnation temperature of 295 K. Recently, Alexeenko *et al.* [14] studied transient flow analysis in micronozzle using the DSMC technique and found that the predicted thrust and mass discharge coefficient decrease with time. Other related studies of gas flows in micronozzles include those reported in References [15–19].

For micro and nano propulsion applications, the nozzle throat diameter is usually less than 1 mm, whereas the stagnation pressure magnitude is of several torrs. A decrease in nozzle throat diameter could result in flows in the micronozzle changing from continuum flow regime to slip flow regime, even transitional or molecular flow regime, depending upon the value of the Knudsen number.

DOI: 10.1002/fld

Although the geometric effect has got the attention of many researchers in the past, the available data are within very limited ranges of Reynolds number and throat diameter for micronozzles [20].

In this paper, numerical simulations were carried out to investigate the gas flow characteristics in an axisymmetric micronozzle configuration within parameter ranges different from previous studies. The emphasis of this paper is on the effect of throat diameter covering a range of macro to micro scales, on the nozzle's performance. For geometric scaling, the nozzle throat diameter was varied from 10 mm (10 000 μm) to 0.1 mm (100 μm). The throat Reynolds number was varied from 5 to 2000. A correlation was developed to predict the specific impulse for helium propellant as a function of throat diameter and throat Reynolds number for design applications. Specific impulse for a selected group of gases was also examined.

2. NUMERICAL STUDY

2.1. Physical problem

Figure 1 shows the schematic geometry of the conical nozzle. The region inside the nozzle, excluding the wall of finite thickness, is of concern for flow calculations. When the throat diameter is less than 1 mm, it is considered as a micronozzle, in which the Reynolds number based on the throat diameter is expected to be much lower than the macro scale nozzles. Owing to the nozzle's symmetrical character, the flow inside the nozzle can be considered as axisymetrical. The typical nozzles investigated in this study have half converging and diverging angles of 30 and 20°, respectively. Based on these parameters, the expansion ratio (ε) of the nozzle is estimated to be 62.41. The ratio of the nozzle length to the exit diameter is 1.354.

The working gas, which is compressible, flows from converging section, throat and diverging section to the nozzle exit. Experimental conditions of Jamison and Ketsdever [13] have been adopted as a basis for geometric scaling and other parametric studies. The gases used in this investigation are helium, nitrogen, argon and carbon dioxide. In the parametric studies, the expansion ratio and converging and diverging angles were fixed.

2.2. Governing equations

In this study, the gas flows through the nozzles with an inlet Knudsen number, *Kn*, less than 0.1. Within this range of Knudsen number, N-S continuum model is valid, which covers both slip and

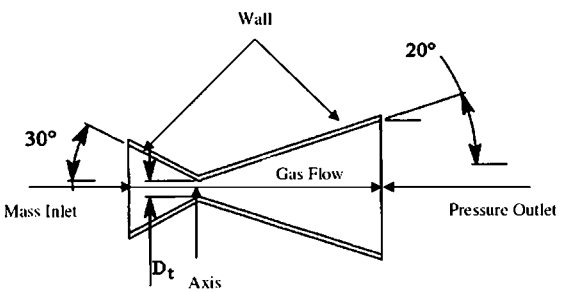

Figure 1. Nozzle geometry.

DOI: 10.1002/fld

no-slip flow regimes. For steady-state, axisymmetric and compressible flows, the N-S equations in cylindrical coordinate system are derived as [21]

Continuity equation:

$$\frac{\partial}{\partial x}(\rho v_x)+\frac{\partial}{\partial r}(\rho v_\mathrm{r})+\frac{\rho v_\mathrm{r}}{r}=0 \tag{1}$$

Axial momentum equation:

$$\frac{1}{r}\frac{\partial}{\partial x}(r\rho v_x v_x)+\frac{1}{r}\frac{\partial}{\partial r}(r\rho v_\mathrm{r} v_x)=-\frac{\partial p}{\partial x}+\frac{1}{r}\frac{\partial}{\partial x}\left[r\mu\left(2\frac{\partial v_x}{\partial x}-\frac{2}{3}(\nabla\cdot\mathbf{v})\right)\right]+\frac{1}{r}\frac{\partial}{\partial r}\left[r\mu\left(\frac{\partial v_x}{\partial r}+\frac{\partial v_\mathrm{r}}{\partial x}\right)\right] \tag{2}$$

Radial momentum equation:

$$\frac{1}{r}\frac{\partial}{\partial r}(r\rho v_\mathrm{r} v_\mathrm{r})+\frac{1}{r}\frac{\partial}{\partial x}(r\rho v_\mathrm{r} v_x)=-\frac{\partial p}{\partial r}+\frac{1}{r}\frac{\partial}{\partial r}\left[r\mu\left(2\frac{\partial v_\mathrm{r}}{\partial x}-\frac{2}{3}(\nabla\cdot\mathbf{v})\right)\right]-\frac{2}{3}\mu\frac{v_\mathrm{r}}{r^2}+\frac{2}{3}\frac{\mu}{r}(\nabla\cdot\mathbf{v})+\frac{1}{r}\frac{\partial}{\partial x}\left[r\mu\left(\frac{\partial v_x}{\partial r}+\frac{\partial v_\mathrm{r}}{\partial x}\right)\right] \tag{3}$$

where

$$\nabla\cdot\mathbf{v}=\frac{\partial v_x}{\partial x}+\frac{\partial v_\mathrm{r}}{\partial r}+\frac{v_\mathrm{r}}{r}$$

Energy equation:

$$\begin{aligned}&\frac{1}{r}\frac{\partial}{\partial r}\left[r\left(\rho C_v T v_\mathrm{r}+p_\mathrm{r}v_\mathrm{r}-v_\mathrm{r}\left[2\mu\frac{\partial v_\mathrm{r}}{\partial r}+\frac{2\mu}{3}\left(\frac{1}{r}\frac{\partial(r v_\mathrm{r})}{\partial r}+\frac{\partial v_x}{\partial x}\right)\right]-v_x\mu\left(\frac{\partial v_x}{\partial r}+\frac{\partial v_\mathrm{r}}{\partial x}\right)-k\frac{\partial T}{\partial r}\right)\right]\\&+\frac{\partial}{\partial x}\left[\left(\rho C_v T v_x+p_x v_x-v_x\left[2\mu\frac{\partial v_x}{\partial x}+\frac{2\mu}{3}\left(\frac{1}{r}\frac{\partial(r v_\mathrm{r})}{\partial r}+\frac{\partial v_x}{\partial x}\right)\right]\right.\right.\\&\left.\left.-v_\mathrm{r}\mu\left(\frac{\partial v_x}{\partial r}+\frac{\partial v_\mathrm{r}}{\partial x}\right)-k\frac{\partial T}{\partial x}\right)\right]=0\end{aligned} \tag{4}$$

Equation of state:

$$\rho=\frac{P}{RT} \tag{5}$$

here, the working fluid is assumed as a perfect gas.

2.3. Boundary conditions

Mass flow rate boundary condition was specified at the inlet. The value of the mass flow rate is determined from a given Re_{throat} along with the stagnation temperature.

DOI: 10.1002/fld

Actual nozzle wall is under complex thermal condition. For simplicity, the nozzle wall was assumed to be under adiabatic thermal conditions in this study:

$$q_w = 0 \tag{6}$$

As the nozzle exit was exposed to near vacuum conditions in the experimental work [13], the exit pressure (P_e) of the nozzle was maintained at a pressure of 10^{-4} torr. The pressure at the nozzle exit [13] was used for calculations as long as the flows were subsonic. If the flow becomes supersonic, all the dependent variables were extrapolated from the interior of the computational domain.

For no-slip flows, the velocity of the fluid ($v_g = 0\,\text{m/s}$) is zero at the walls. For slip flows, the velocity slip and the temperature jump derived by Maxwell were used [14]:

$$v_w - v_g = \left(\frac{2-\alpha_v}{\alpha_v}\right) Kn \frac{\partial v}{\partial n} + \frac{3}{4}\frac{\mu}{\rho T}\frac{\partial T}{\partial x} \tag{7}$$

$$T_w - T_g = \frac{2\gamma}{(\gamma+1)Pr}\left(\frac{2-\alpha_T}{\alpha_T}\right)\lambda \left.\frac{\partial T}{\partial n}\right|_0 \tag{8}$$

In temperature jump equation (7), the second and third terms on the right-hand side can be combined and an equivalent mean free path was computed as

$$\lambda_T = \frac{4}{\gamma+1}\frac{k}{\rho \bar{c} C_v} = \frac{2}{\gamma+1}\frac{k}{\rho C_v}\sqrt{\frac{\pi}{2RT}} \tag{9}$$

Hence, Equation (7) reduces to the following form:

$$T_w - T_g = \left(\frac{2-\alpha_T}{\alpha_T}\right)\lambda_T \left.\frac{\partial T}{\partial n}\right|_0 \tag{10}$$

The slip boundary conditions have been specified depending on the value of the Knudsen number, which is defined as the ratio of the mean free path (λ) of the gas to the characteristic dimension of the flow geometry (L):

$$Kn = \frac{\lambda}{L} \tag{11}$$

In this paper, the characteristic dimension is the throat diameter.

2.4. Numerical computations

Numerical simulations have been carried out using the commercial CFD code FLUENT [22], which is based on the cell-centered finite volume approach. All governing equations were discretized by the second-order upwind scheme for acceptable accuracy. Discretized continuity, momentum and energy equations were solved in segregated solver with conjunction of algebraic multigrid method. For pressure–velocity coupling, SIMPLE algorithm was used [23]. The solution was declared as converged when the residual for each variable becomes less than the chosen convergence criterion. In present simulations, the convergence criteria for velocity, pressure and energy are set to a value of 10^{-6} for no-slip flows, whereas it was 10^{-7} for slip flows.

The computational domain was meshed with quadrilateral elements with map scheme to yield a regular, structured grid. The grid nodes were placed in such a way that there were enough nodes near the throat and wall regions in order to capture the higher variable gradient accurately.

DOI: 10.1002/fld

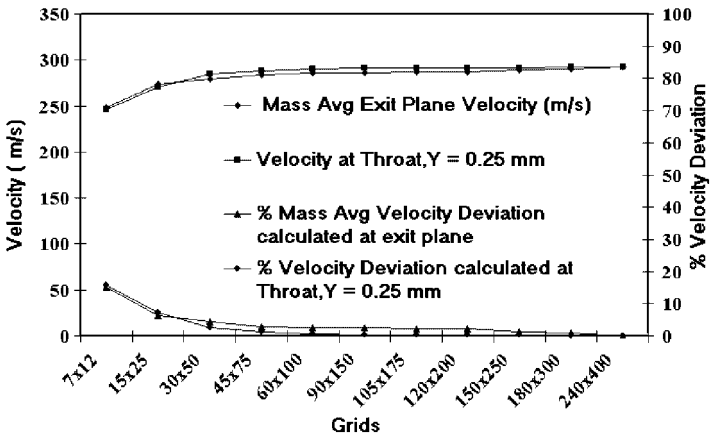

Figure 2. Grid independence study.

Grid independence test has also been carried out by evaluating the change of the mass-averaged velocity at the exit plane of the nozzle and that of velocity at a selected point in the throat. The coordinates of one of the selected points used for this purpose were 1.221e−3 and 0.25e−3. Based on numerical computations, a number of 240×400 grid points were found to be fully enough for the numerical computation. Hence, this mesh size has been used as the reference grid to calculate the percentage deviation of velocities for a mesh size of 7×12–240×400.

Figure 2 shows the results of grid independence tests, where left-hand scale denotes the velocity (m/s) and the right-hand scale represents the percentage of the velocity deviation from the finest grid. It can be observed that at a grid number of 150×250, the percentage deviation in the mass-averaged exit velocity from the finest grid was about 1.4% and that for the velocity at throat, x (or Y in the figure) $= 0.25$ mm, was only 0.1624%. Therefore, 150×250 has been considered as the optimum number of grid number for all of the numerical simulations.

3. RESULTS AND DISCUSSION

3.1. Comparison with available data

The nozzle exit thrust is usually defined as the sum of velocity thrust ($M_e V_e$) and pressure thrust ($P_e A_e$) and is given by the following equation:

$$T_n = M_e V_e + P_e A_e \tag{12}$$

Figure 3 shows the results of numerical simulations using current model and comparisons with available experimental data of Jamison and Ketsdever [13]. Calculations of exit thrust were carried out with and without the pressure component for both slip and no-slip boundary conditions. It can be observed from the figure that the numerical results of nozzle exit thrust without pressure component agree fairly well with the experimental data. The numerical results also predict the trend of variation in exit thrust with the change in the throat Reynolds numbers. Within the investigated

DOI: 10.1002/fld

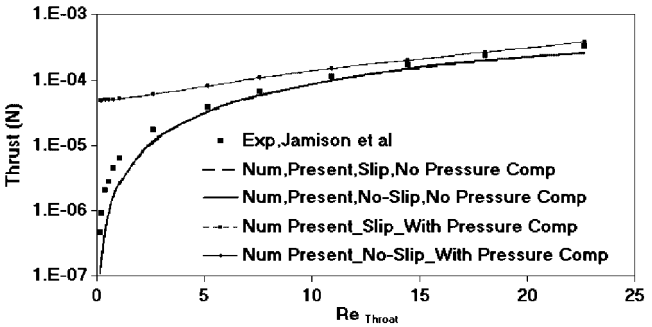

Figure 3. Comparisons of numerical results with experimental data.

Reynolds number range, the no-slip boundary condition predicts slightly higher value in the exit thrust than the slip flow condition does.

3.2. Flow and thermal fields

Figure 4 shows the velocity profiles at the throat (a and b) and exit (c and d) of the micronozzle with no-slip and slip boundary conditions, respectively. Helium was the working fluid. The coordinates in throat and exit have been normalized by throat radius (R_t) and exit radius (R_e), respectively. Difference in thrust between slip and no-slip boundary conditions is found to be very small. The velocity profile difference between these two flow conditions near the wall regions is found significant, especially when considering the fact that the velocity on the wall is not zero for slip boundary condition. The slip velocity on the walls increases with increase in Reynolds numbers. At very low Reynolds numbers, the velocity profiles tend to become flatter in the vertical direction, whereas velocity profiles become more parabolic at higher Reynolds numbers. In the latter scenario, the maximum value of the velocity occurs at the center of the nozzle for both slip and no-slip conditions.

Figure 5 shows the Mach number distribution in the form of iso-contours inside the micronozzle at low values of Reynolds numbers ($Re_{\text{throat}} = 0.164$ and 0.549) under slip and no-slip boundary conditions. The major difference between the slip and no-slip computation is observed near the wall region, with the no-slip conditions predicting higher value of Mach number near the wall region. It is also noticed that the no-slip flow condition can produce higher local Mach values than the slip flow condition near the center of the nozzle exit. The high Mach number zone near the nozzle throat for slip flow condition is found slightly higher than that for no-slip flow condition especially when Reynolds numbers are relatively lower.

Comparison of the contours of static pressures shows that the pressure distributions in the micronozzles are almost identical for slip and no-slip boundary conditions at different Reynolds numbers. Figure 6 shows the comparison of the static pressure contours in the micronozzle at $Re_{\text{throat}} = 0.549$ for both slip and no-slip boundary conditions. In general, there is a gradual variation in static pressure from inlet to throat, and after that static pressure decreases drastically up to the exit of the micronozzle.

Figure 7 shows the static temperature contours in the micronozzles at both slip and no-slip boundary conditions for $Re_{\text{throat}} = 0.549$ and 7.582. It can be observed that the areas of lower temperatures are located near the throat and exit. At lower Reynolds numbers, the variation in the

DOI: 10.1002/fld

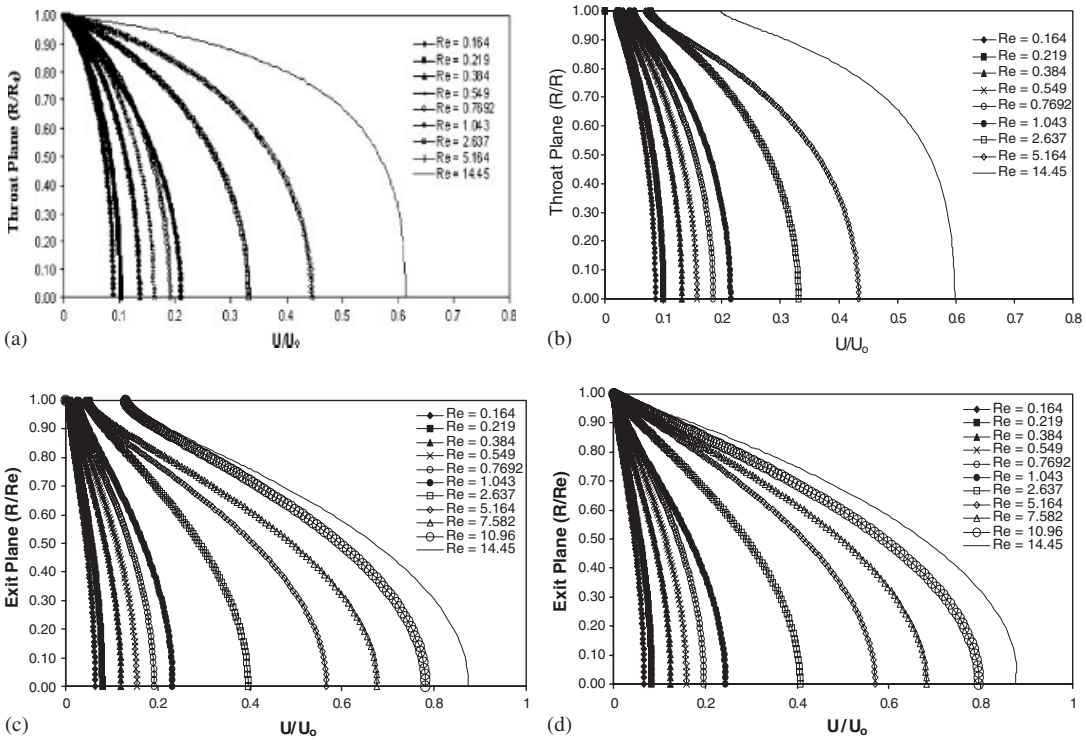

Figure 4. Velocity profiles at nozzle throat and exit with slip and no-slip boundary conditions: (a) at throat, no-slip; (b) at throat, slip; (c) at exit, slip; and (d) at exit, no-slip.

temperature in the nozzle is also of a very low order (± 3 K). Although, the temperature patterns at lower Reynolds number for slip and no-slip boundary conditions are almost identical, but the area of higher temperature zone near the wall region is more predominant for slip flows than those for no-slip flows at higher Reynolds numbers ($Re_{\text{throat}} > 1.043$). Compared with the effects of slip boundary condition (as shown in Figures 7(a) and (b)), the effects of the throat Reynolds number on the temperature field (as indicated in figures (c) and (d)) were found to be more significant. This is because the Reynolds number increase has caused larger and more massive change in the gas's kinetic energy and thermal field, whereas slip boundary condition effects are more sensitive in the near-wall region.

3.3. Specific impulse

The specific impulse, I_{sp}, is a measure of the velocity thrust per weight of gas or propellant, which can be expressed as:

$$I_{\text{sp}} = \frac{V_{\text{e}}}{g} \tag{13}$$

The following calculations of specific impulse are based on no-slip boundary conditions. Figure 8 shows the variation in specific impulse (I_{sp}), as a function of throat diameter (D_{t}), at various

DOI: 10.1002/fld

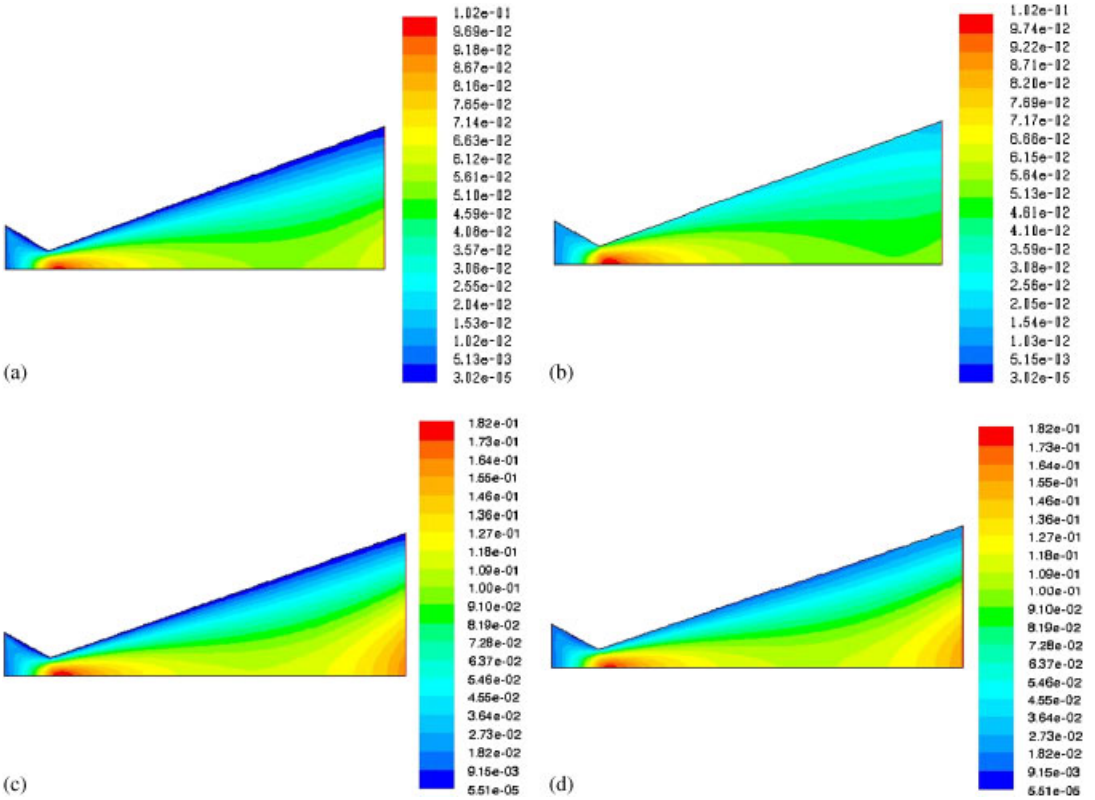

Figure 5. Mach number contours at slip and no-slip boundary conditions for $Re_{\text{throat}} = 0.164$ and 0.549: (a) $Re_{\text{throat}} = 0.164$, no-slip; (b) $Re_{\text{throat}} = 0.164$, slip; (c) $Re_{\text{throat}} = 0.549$, no-slip; and (d) $Re_{\text{throat}} = 0.549$, slip.

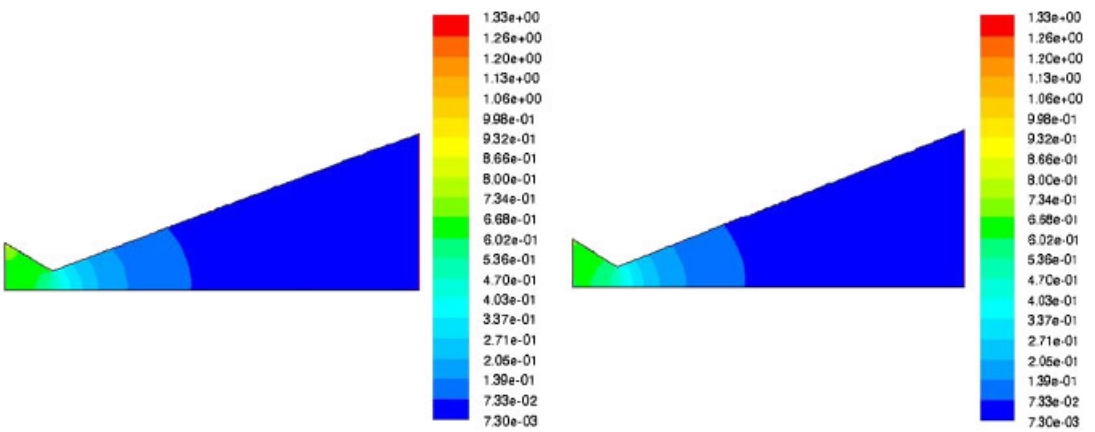

Figure 6. Static pressure contours (torr) at slip and no-slip boundary conditions for $Re_{\text{throat}} = 0.549$.

DOI: 10.1002/fld

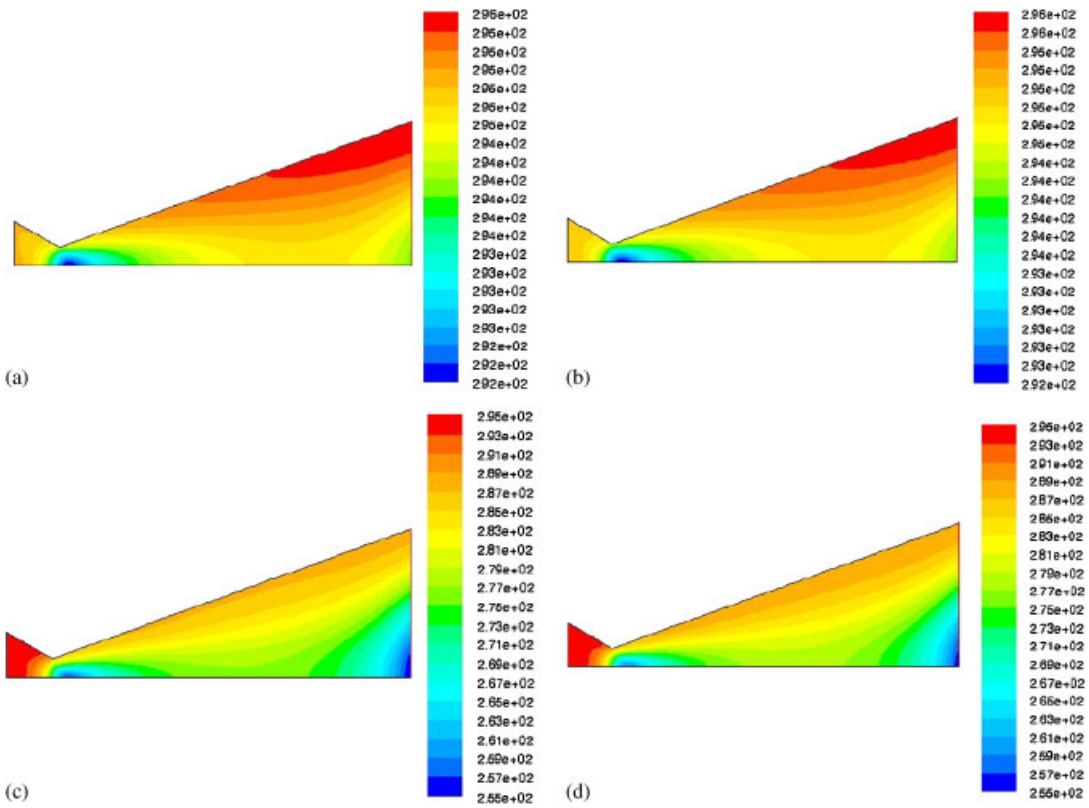

Figure 7. Static temperature contours (Kelvin) at slip and no-slip boundary conditions for $Re_{\text{throat}} = 0.549$ and 7.582: (a) $Re_{\text{throat}} = 0.549$, no-slip; (b) $Re_{\text{throat}} = 0.549$, slip; (c) $Re_{\text{throat}} = 7.582$, no-slip; and (d) $Re_{\text{throat}} = 7.582$, slip.

Reynolds numbers based on throat diameter (Re_{throat}). It can be observed that for each Re_{throat}, with the decrease in D_t from macro scale to micro scale, there is a fixed D_t (turning point) beyond which the increase in I_{sp} is marginal or near-flat. There is also a shift of the turning point with the increase of Re_{throat} due to the nonlinear effects of geometric dimension on I_{sp}. These tuning points were matched with a smooth curve that divides the plots into two zones, namely scale sensitive region and scale numb region. The variation in I_{sp} with D_t is much more rapid in the scale sensitive region than in the scale numb region. In micro scale, the variations in I_{sp} with D_t fall into the scale sensitive region, indicating that micronozzles are highly sensitive to throat diameters than macro scale nozzles.

Based on the present parametric investigation, a correlation has also been developed, on the basis of summarizing the simulations results, to calculate the variation in specific impulse at any given throat diameter (D_t) and throat Reynolds number (Re) for helium propellant:

$$I_{sp} = C\, Re^{1/3} D_t^{-2.04} \tag{14}$$

where C is a constant and can be approximated to be 29.54. Figure 9 shows the plot for variation in specific impulse (using the above correlation) with throat diameters at various throat Reynolds

DOI: 10.1002/fld

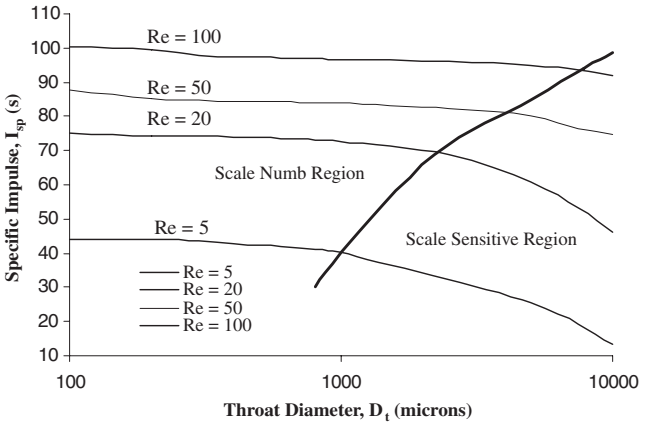

Figure 8. Variation in specific impulse with the variation in throat diameter for different throat Reynolds numbers ($Re = Re_{\text{throat}}$).

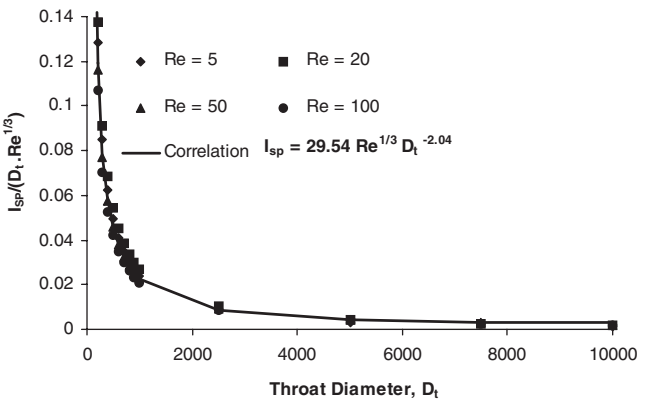

Figure 9. Correlation for specific impulse as a function of throat diameter (in microns) and throat Reynolds number ($Re = Re_{\text{throat}}$).

numbers. Using the format of $I_{\text{sp}}/(D_{\text{t}}\,Re^{1/3})$ vs D_{t}, all numerical data at different Reynolds numbers and throat diameters can be fitted into a single curve. It is estimated that the correlation developed above can predict specific impulse of helium propellant at any given throat diameter and Reynolds number within an average error of 10%.

Figure 10 shows a comparison of specific impulse for different gases (helium, nitrogen, argon and carbon dioxide) at throat diameters of 0.1 mm. These gases are selected because of their potential applications in micronozzles. During the computational simulation, the values of the thermophysical properties were changed for different gases. From Figure 10, it can be seen that helium is the best propellant among the other gases studied for specific impulse generation. At a higher Reynolds number, significant difference in specific impulse among the gases has been observed. The relative trends of variation in specific impulse with Reynolds number for the four propellants are found to be very similar at both micro scale and macro scale nozzles.

DOI: 10.1002/fld

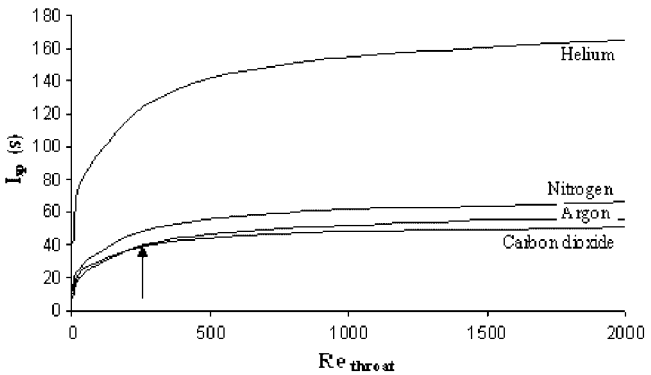

Figure 10. Variation of specific impulse for different propellants at different Re_{throat}. $D_t = 0.1$ mm.

4. CONCLUSIONS

Numerical simulations for gas flows in micronozzles under slip and non-slip conditions have been conducted. It is found that velocity profiles at the throat and exit possessed parabolic nature; however, velocity distributions in the near-wall regions are quite different for slip and no-slip conditions. Under the same conditions, micronozzles can produce higher local Mach numbers and lower temperature in the near-wall region of the divergent section and the exit.

Variation in I_{sp} was found to be negligible within the throat diameter range from 1 to 0.1 mm when compared with that from 10 to 1 mm for a given throat Reynolds number. A correlation for prediction of specific impulse based on throat diameter and throat Reynolds number was developed within an average error of 10%. Helium has proved to be the best propellant for specific impulse generator in micronozzles among the other four propellants investigated.

NOMENCLATURE

A_e	exit area (m^2)
C_v	specific heat at constant volume
D_t	throat diameter (m)
k'	Boltzmann's constant (1.38e−23 J/K)
k	thermal conductivity (W/m K)
Kn	Knudsen number
I_{sp}	specific impulse (s)
L	characteristic length (m)
M_e	flow rate (kg/s)
P	static pressure (Pa)
P_e	exit pressure (Pa)
P_0	stagnation pressure (torr)
p_x	axial pressure (Pa)
p_r	radial pressure (Pa)
q	heat flux (W/m^2)

DOI: 10.1002/fld

r	radial coordinate (m)
R	gas constant (kJ/kg K)
Re_{throat}	throat Reynolds number
R_{t}	throat radius (m)
R_{e}	exit radius (m)
T	static temperature (K)
T_0	stagnation temperature (K)
T_{w}	wall temperature (K)
T_{n}	nozzle exit thrust (N)
V_{e}	exit velocity (m/s)
v_x	axial velocity (m/s)
v_{r}	radial velocity (m/s)
x	axial coordinate (m)

Greek symbols

λ	mean free path (m)
σ	collision diameter of the molecules (m)
α_v	momentum accommodation coefficient
α_{T}	thermal accommodation coefficient
μ	molecular viscosity (kg/m s)
ρ	fluid density (kg/m^3)
ε	expansion ratio

Subscripts

e	exit
g	gas
n	nozzle
0	stagnation
r	radial
t	throat
w	wall

ACKNOWLEDGEMENTS

The authors would like to acknowledge the Air Force Office of Scientific Research (AFOSR) for supporting this research under contract No.: F49620-03-1-0314. Thanks also to Mr. Rajesh Singh for his assistance in preparing the manuscript.

REFERENCES

1. Rothe DE. Electron beam studies of viscous flow in supersonic nozzle. *AIAA Journal* 1971; **9**(5):804–810.
2. Ivanov MS, Markelov GN, Ketsdever AD, Wadsworth DC. Numerical study of cold gas micronozzle flows. *AIAA-1999-166*, 1999.
3. Kim SC. Calculations of low-Reynolds number resistojet nozzles. *Journal of Spacecraft and Rockets* 1994; **31**(2):259–264.
4. Chung CH, Kim SC, Stubbs RM, DeWitt KJ. Low density nozzle flow by direct simulation Monte Carlo and continuum methods. *Journal of Propulsion and Power* 1995; **11**(1):64–70.

DOI: 10.1002/fld

5. Zeleznik D, Micci MM, Long LN. Direct simulation Monte Carlo model of low Reynolds number nozzle flows. *Journal of Propulsion and Power* 1994; **9**(4):546–553.
6. Choudhuri AR, Baird B, Gollahalli SR, Schneider SJ. Effects of geometry and ambient pressure on micronozzle flow. *AIAA-2001-3331*, 2001.
7. Boyd ID, Penko PF, Meissner DL, Dewitt KJ. Experimental and numerical investigations of low density nozzle and plume flows of nitrogen. *AIAA Journal* 1992; **30**(10):2453–2461.
8. Bayt RL. Analysis, fabrication and testing of a MEMS-based micro propulsion system. *Ph.D. Thesis*, Massachusetts Institute of Technology, Cambridge, MA, 1999.
9. Menzies RDD, Richards BE, Badcock KJ, Loseken, Kahl M. Computational investigation of three-dimensional flow effects on micronozzles. *Journal of Spacecraft and Rockets* 1999; **39**(4):642–644.
10. Rossi C, Rouhani MD, Esteve D. Prediction of the performance of a Si-micromachined micro thruster by computing the subsonic gas flow inside the thruster. *Sensors and Actuators*, *Physical A* 2000; **87**:96–104.
11. Raju R, Pandey BP, Roy S. Finite element model of fluid flow inside a micro-thruster. *AIAA-2002-573*, 2002.
12. Ivanov MS, Markelov GN, Kashkovsky AV. Numerical analysis of thruster plume interaction problems. In *Proceedings of the 2nd European Spacecraft Propulsion Conference*, Perry M (ed.). European Space Agency: Paris, 1997; 603–610.
13. Jamison AJ, Ketsdever AD. Low Reynolds number performance comparison of an under expanded orifice and a DeLaval nozzle. *Proceedings of the 23rd International Symposium on Rarefied Gas Dynamics*. American Institute of Physics: Melville, NY, 2003; 557–564.
14. Alexeenko AA, Fedosov DA, Gimelshein SF, Levin DA, Collins RJ. Transient heat transfer and gas flow in a MEMS-based thruster. *Journal of Microelectromechanical Systems* 2006; **15**(1):181–194.
15. Thornber B, Chesta E, Gloth O, Brandt R, Schwane R, Perigo R, Smith P. Numerical simulation of micronozzles with comparison to experimental results. *Proceedings of the 4th International Spacecraft Propulsion Conference* (*ESA SP-555*), Sardinia, Italy, 2004; 773–778.
16. Borovkov AI, Pyatishev EN, Lurie MS, Korshunov AV, Akulshin YD, Dolganov AG, Sabadash VO. Micronozzles: 3D numerical structural and gas dynamics modeling, fabrication and preliminary experimental results. *Proceedings of the 4th International Workshop on Nondestructive Testing and Computer Simulations in Space Science and Engineering*, vol. 4348, 2001; 348–354.
17. Rossi C, Do Conto T, Esteve D, Larangot B. Design, fabrication and modeling of MEMS-based microthrusters for space application. *Smart Materials and Structures* 2001; **10**:1156–1162.
18. Zhang KL, Chou AK. Performance prediction of a novel solid-propellant microthruster. *Journal of Propulsion and Power* 2006; **22**(1):56–63.
19. Liu M, Zhang X, Zhang G, Chen Y. Study on micronozzle flow and propulsion performance using DSMC and continuum methods. *Acta Mechanica Sinica* 2006; **22**:409–416.
20. Hao PF, Ding YT, Yao ZH, He F, Zhu KQ. Size effect on gas flow in micro nozzles. *Journal of Micromechanics and Microengineering* 2005; **15**:2069–2073.
21. Gadepalli VVV. Numerical simulation of gas flows in a De-Laval micro nozzle. *M.S. Thesis*, Florida International University, Miami, FL, 2005.
22. Fluent Inc. *FLUENT Users Guide v 6.1*, Lebanon, NH, 2003.
23. Patankar SV. *Numerical Heat Transfer and Fluid Flow*. Hemisphere Publication Company: New York, 1980.

DOI: 10.1002/fld